

lated to the matrix elements \mathcal{P}_0 for $M=0$ by

$$\mathcal{P}_M^2/\mathcal{P}_{M=0}^2 = 1 - M^2/J^2. \quad (4)$$

These equations have been programmed for a digital computer by Rhodes and Hopf⁶ using numerical integration of the density-matrix equations. Computer runs were made for our case, taking into account the degeneracy of the CO₂ transitions. A uniform-intensity plane wave was assumed with a diameter of 8.5 mm (the amplifier aperture size). Diffraction effects were ignored, the average value of intensity along the beam being used. The parameters used in the computation, corresponding to the experimental conditions, were $T_2 = 85$ nsec (at a pressure of 0.8 Torr), exponential gain coefficient 0.32 m^{-1} , Doppler width 60 MHz, and the matrix elements appropriate to the CO₂ transition. The curve labeled "theoretical" in Fig. 1 was obtained. The agreement is reasonably good, in spite of the fact that variations of intensity along the length of the amplifier due to diffraction and refocusing were ignored in the computation.

Apart from their theoretical interest, the ef-

fects described here have possible practical application to the production of very short and intense radiation pulses at 10- μm wavelength.

The authors gratefully acknowledge the use of the computer program developed by Dr. C. K. Rhodes, and experimental advice provided by Dr. C. K. Cheo.

*Work supported in part by the Air Force Cambridge Research Laboratories, Office of Aerospace Research under Contract No. F19628-70-C-0064, and in part by the Joint Services Electronics Program, Contract No. DA28-043-AMC-02536(E).

¹C. K. N. Patel and R. E. Slusher, *Phys. Rev. Lett.* **19**, 1019 (1967).

²C. Hocker and C. Tang, *Phys. Rev. Lett.* **21**, 591 (1968).

³T. J. Bridges and P. K. Cheo, *Appl. Phys. Lett.* **14**, 262 (1969).

⁴H. Kogelnik and T. J. Bridges, *IEEE J. Quantum Electron.* **95** (1967).

⁵F. A. Hopf and M. O. Scully, *Phys. Rev.* **179**, 399 (1969).

⁶F. A. Hopf, C. K. Rhodes, and A. Szöke, "Influence of Degeneracy on Coherent Pulse Propagation in an Inhomogeneously Broadened Laser Amplifier" (to be published).

OBSERVATION OF SIMULTANEITY IN PARAMETRIC PRODUCTION OF OPTICAL PHOTON PAIRS

David C. Burnham and Donald L. Weinberg

National Aeronautics and Space Administration Electronics Research Center, Cambridge, Massachusetts 02142

(Received 12 May 1970)

The quantum mechanical description of parametric fluorescence is the splitting of a single photon into two photons. This description has been verified by observing coincidences between photons emitted by an ammonium dihydrogen phosphate crystal pumped by a 325-nm He-Cd laser. The coincidence rate R_C decreases to the calculated accidental rate [$<0.03R_C(\text{max})$], unless the two detectors are arranged to satisfy energy and momentum conservation and have equal time delays.

In the elementary quantum process of decay of a photon (ω_p) into two new photons (ω_1, ω_2), emission of the products should be simultaneous¹:

$$t_1 = t_2. \quad (1)$$

The decay is allowed in a medium which lacks inversion symmetry. If the medium is invariant to translations in space and time, momentum and energy must be conserved:

$$\vec{k}_p = \vec{k}_1 + \vec{k}_2, \quad (2)$$

$$\omega_p = \omega_1 + \omega_2. \quad (3)$$

This process is called² parametric fluorescence, parametric scattering, or parametric noise, and (2) and (3) are already well known as the phase-

matching conditions. We have verified that photon coincidence occurs unless any of the conditions of (1)-(3) is violated.

The optical arrangement is illustrated in Fig. 1. Phase matching was satisfied by using the birefringence of an ADP crystal, $L = 25$ mm long, whose optic axis made an angle of 52.4° with the normal to the faces. The pump was the 325-nm beam of a He-Cd laser (Spectra-Physics model No. 185) with single-isotope cadmium, power $P_p = 9$ mW, and about 2-mm beam diameter. Phase matching requires that the two new beams, to be at visible frequencies, be of ordinary polarization. It follows that each new frequency is emitted in a cone at angle $\phi_{1,2}$ around the pump beam.

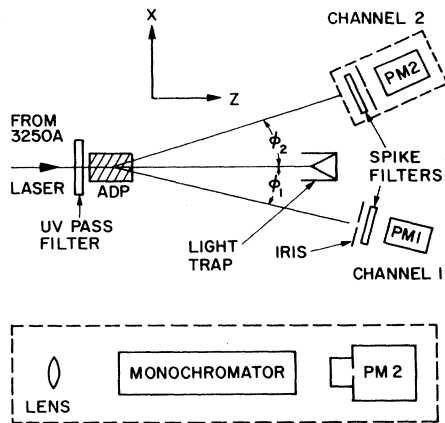


FIG. 1. Experimental arrangement. All components except the aperture in channel 1 are nominally centered on the horizontal (XZ) plane. There are sharp-cut filters in each channel to suppress scattered uv light and fluorescence. Channel 1: The aperture is located 1.00 m from the center of the crystal, and can be translated in the transverse (XY) plane. The spike filter has peak transmittance of 74% at 633 nm, and 4.0-nm pass band. The photomultiplier is an Amperex 56TUVP, with S-20 cathode apertured to 25 mm diam, and dark counting rate of 1600 sec^{-1} . Channel 2: The upper dashed-line box is symbolic. The actual arrangement is shown in the lower dashed-line box. A 95-mm focal length lens, 1.1 m from the crystal, images the pump beam position in the crystal onto the entrance slit of a $\frac{1}{4}$ -m Jarrell-Ash monochromator. The beam emerging from the exit slit travels 50 mm and then strikes the photocathode of an FW-130 photomultiplier, an S-20 type, with 35-sec^{-1} dark counting rate, whose sensitive cathode area is only 1 mm in diameter. The effective aperture at the lens is therefore 2 mm in diameter. The monochromator slits are 0.5 mm wide, giving a bandwidth of 1.5 nm.

$\varphi_{1,2}$ depends upon the angle θ of pump propagation with respect to the optic axis. As shown³ for $\omega_p = 347 \text{ nm}$, $\varphi_{1,2}$ at constant θ is a slowly varying function of $\omega_{1,2}$ near the subharmonic frequency, except at very small φ . Thus the two coincident photons and the pump all travel in a common plane, and $\varphi_1 \approx \varphi_2$. The calculated variation of φ_1 with θ for red light was confirmed by visual observation.

Coincidence rates were measured with a photomultiplier in each channel, as illustrated in Fig. 1. Each photomultiplier is followed by a fast $\times 1000$ amplifier, and an EG & G T105/N discriminator, whose output pulse length (nominally 19.5 nsec) is determined by a cable. Pulses from the two discriminators are combined in an EG & G C102B/N AND logic unit to detect coincidences. The counting rate of each channel, R_1

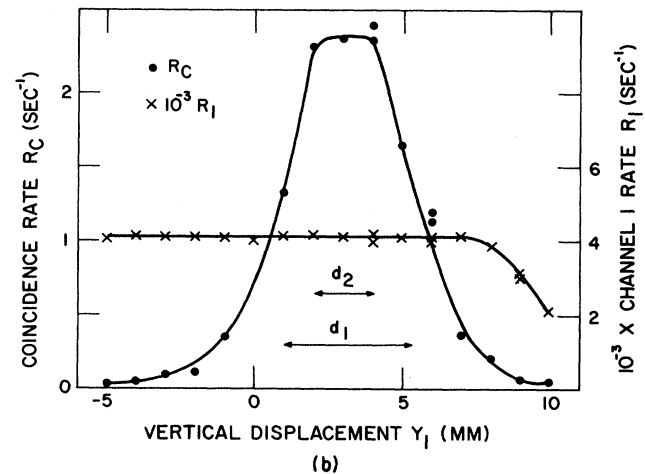
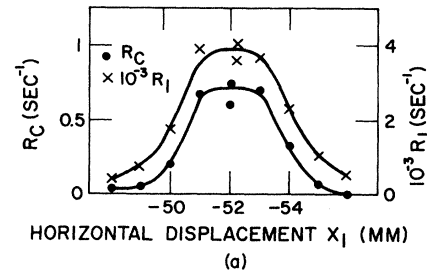


FIG. 2. R_C and R_1 as functions of position of aperture 1, for $\lambda_2 = 668.5 \text{ nm}$ and time delay $\tau = 0$; counting time 100 sec. (a) Horizontal (X_1) scan for $Y_1 = 0$. The pump beam position is $X_1 = 0$. (b) Vertical (Y_1) scan for $X_1 = -52 \text{ mm}$. The nominal plane of the apparatus is $Y_1 = 0$. The aperture diameters, $d_1 = 4.3$ and $d_2 = 2 \text{ mm}$ for the two channels, are illustrated. $R_2 = 260 \text{ sec}^{-1}$. Here R_1 and R_2 have been corrected for dark counts. R_C has not been corrected for the calculated accidental counting rate [0.06 sec^{-1} in (b) in the range where R_1 is constant].

and R_2 , and the coincidence rate R_C are recorded by SEN-312 scalers which respond to 3-nsec pulses.

In setting up the experiment, we fixed $\lambda_1 = 633 \text{ nm}$, $\lambda_2 = 668 \text{ nm}$, and $\varphi_2 \approx 50 \text{ mrad}$ (external to the crystal), and chose a small aperture for detector 2. Phase matching was attained by adjusting θ for maximum counting rate R_2 in channel 2. A larger aperture was used in channel 1 to be sure of accepting all the photons which were partners of those observed in channel 2. These partners were located by scanning the aperture over the large sensitive surface of detector 1. Figure 2 shows the results of (a) horizontal and (b) vertical scans at $\theta = 56.2^\circ$ (internal). The variation of R_1 in (a) shows the sharp phase-matching peak for scanning perpendicular to the emission circle. Since the background is low,

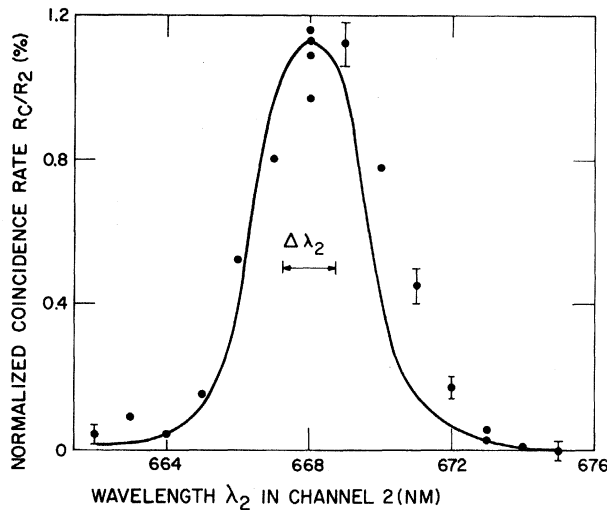


FIG. 3. Normalized coincidence rate R_C/R_2 vs λ_2 . The dark count and calculated accidental coincidence rates have been subtracted. The solid-line curve is the response predicted by Eq. (3), based on the transmittance of the spike filter in channel 1, and normalized to the peak coincidence rate, but uncorrected for finite $\Delta\lambda_2$. The channel 1 aperture was 10 mm in diameter and centered at $X_1=Y_1=0$. The R_2 peak (not shown) was several times wider than the R_C/R_2 peak, since the variation of φ_2 with λ_2 is slow. $R_1 = 1.1 \times 10^4 \text{ sec}^{-1}$ (corrected).

most of R_1 arises from parametric fluorescence. By the same test, R_2 was entirely due to parametric fluorescence. In Fig. 2(a) the peak center at -52 mm corresponds to φ_1 (external) = 52 mrad , φ_1 (internal) = 34 mrad . Then φ_2 (internal) = 36 mrad is calculated. For scanning tangentially to the emission circle, Fig. 2(b), R_1 is constant as expected, except for the decrease at large Y which simply results from scanning off detector 1. In Fig. 2(a) the coincidence rate R_C varies much as does R_1 . However, in Fig. 2(b) R_C is strongly peaked even though R_1 is constant, thus verifying conservation of momentum [Eq. (2)] in the vertical direction.

Figure 3 shows the variation of R_C with λ_2 , normalized to R_1 to compensate for the variation of R_1 with λ_2 . Except for a small error in wavelength calibration, the results agree with the predictions of energy conservation, Eq. (3).

Figure 4 shows the effect of introducing a relative delay between the two channels. The width of the plateau, or gate time τ_C , is $35 \pm 2 \text{ nsec}$, in reasonable agreement with the value of 33 nsec expected from the electronic circuits. The circuits were adjusted for τ_C , long compared with the minimum value attainable, in order to be

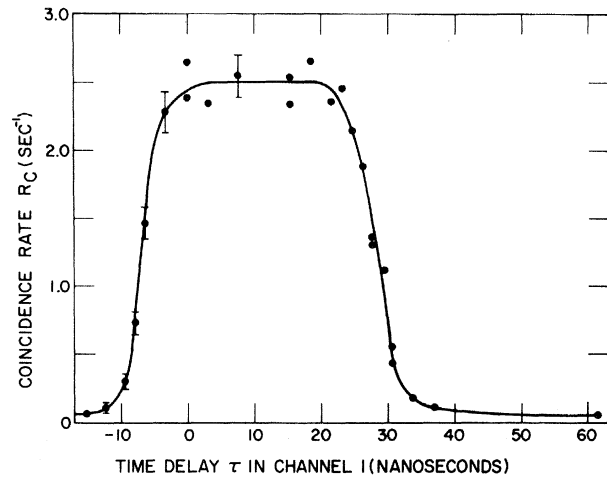


FIG. 4. R_C vs delay τ in channel 1. The delays are introduced by adding cables between the amplifiers and discriminators. The width of the plateau is $35 \pm 2 \text{ nsec}$ full width at half-maximum. The asymmetry of the curve center about $\tau=0$ results from different transit times in the dissimilar photomultipliers and amplifiers. No correction has been made for the calculated accidental coincidence rate, 0.05 sec^{-1} . $R_1=3600$ and $R_2=250 \text{ sec}^{-1}$, with dark counts subtracted. $\lambda_2=668.5$, $X_1=-52$, and $Y_1=3 \text{ mm}$.

sure of observing the maximum coincidence rate. The steepness of the drop in R_C at each end of the plateau in Fig. 4 sets an upper limit on the correlation time τ_C , which denotes how nearly coincident [Eq. (1)] the photons are. The left end is steeper and indicates that $\tau_C \leq 4 \text{ nsec}$, which is a reasonable value of jitter for the photomultipliers and the counting equipment.

The counting rates in channels 1 and 2 are related to the photon arrival rates N_i and quantum efficiencies η_i by $R_i = \eta_i N_i$. For perfect correlation, one expects a maximum coincidence rate $R_C = \eta_1 R_2$, since detector 1 collects the partner of any photon detected by detector 2. Thus when Eqs. (1)-(3) are satisfied the counting rates yield $\eta_1 = (R_C/R_2)_{\text{max}}$, the quantum efficiency of detector 1, including the effects of filters before the detector. We find $\eta_1 = 1.1\%$ in Fig. 3 and $\eta_1 = 1.0\%$ in Figs. 2 and 4. For comparison, direct measurement of the quantum efficiency of detector 1 (including filters), using a calibrated lamp, gave $\eta_1 = 1.35\%$, with an estimated systematic error of $\pm 20\%$. Thus the coincidence measurements show high photon correlation, consistent with 100% correlation. After correction for filters, the correlation measurements lead to $\eta_1 = 2.1\%$ for the 56TUVF alone, in agreement with results by other workers⁴ on a similar tube.

Using η_1 leads to $N_1 = 4 \times 10^5 \text{ sec}^{-1}$ for the photon arrival rate. The same quantity can be calculated theoretically as⁵

$$N_1 = 512\pi^5 h c d_{36}^2 \sin^2 \theta P_p L \csc(\varphi_1 + \varphi_2) \Delta\lambda_1 \Delta\alpha_1 / n_p n_2 \lambda_1^5 \lambda_2 = 8.0 \times 10^5 \text{ sec}^{-1},$$

in reasonable agreement with experiment. Here d_{36} is a nonlinear coefficient of the crystal, θ and φ are internal angles, and $\Delta\alpha_1$ is the angle subtended at the crystal by detector 1.

This experiment has only set an upper bound on τ_C , the deviation from the coincidence condition, Eq. (1). Presumably, a photon can be no better localized in time than the inverse of its bandwidth. Thus the theoretical lower limit of τ_C is the inverse of the smaller bandwidth $\Delta\lambda_2 = 1.5 \text{ nm}$, or $\tau_C = 2 \times 10^{-13} \text{ sec}$. One might possibly expect that τ_C is related to the coherence time of the pump laser. The He-Cd laser oscillates in about 15 longitudinal modes, with a total bandwidth about 10^9 Hz , corresponding to $\tau_C = 2 \times 10^{-10} \text{ sec}$, which is still too small to observe in the present experiment. With a single-mode laser, a coherence time $>100 \text{ nsec}$ is possible, so that one would expect a much smaller coincidence rate if τ_C were really determined by the pump coherence time.

The expected accidental coincidence rate is

$$\begin{aligned} \langle R_C(\text{acc}) \rangle &= \tau_C \langle R_1 R_2 \rangle \\ &= \tau_C \langle R_1 \rangle \langle R_2 \rangle + \tau_C \langle \Delta R_1 \Delta R_2 \rangle \end{aligned} \quad (4)$$

(with backgrounds now included in the R 's). Eq. (4) has been checked in the experiments of Figs. 2(b) and 4, where R_1 and R_2 are kept constant but Eqs. (1) and (2) are violated in order to eliminate real coincidences. In both cases R_C falls to a low level consistent with the first term on the right-hand side of Eq. (4), without any need to invoke the last term, which might arise from fluctuations of pump power. For large τ , $\langle R_C(\text{acc}) \rangle$ was measured more accurately at higher R_1 and R_2 , and agreed with $\tau_C \langle R_1 \rangle \langle R_2 \rangle$ within 10%. The same formula was also verified with a dc-powered incandescent light source. In summary, the maximum observed real coincidence rate was at least 100 times any unexplained residual coincidence rate.

The authors thank N. Knable for encouragement and cooperation, and G. Schappert, E. Sarachik, and B. Mollow for helpful theoretical discussions.

¹Ya. B. Zel'dovich and D. N. Klyshko, *Zh. Eksp. Teor. Fiz.—Pis'ma Red.* **9**, 69 (1969) [*JETP Lett.* **9**, 40 (1969)].

²S. E. Harris, M. K. Oshman, and R. L. Byer, *Phys. Rev. Lett.* **18**, 732 (1967); D. Magde and H. Mahr, *Phys. Rev. Lett.* **18**, 905 (1967); and many later papers.

³D. Magde and H. Mahr, *Phys. Rev.* **171**, 393 (1968).

⁴R. Foord, R. Jones, C. J. Oliver, and E. R. Pike, *Appl. Opt.* **8**, 1975 (1969).

⁵D. A. Kleinman, *Phys. Rev.* **174**, 1027 (1968); D. L. Weinberg, *Appl. Phys. Lett.* **14**, 32 (1969).

FAR-INFRARED OBSERVATION OF ELECTRIC-DIPOLE-EXCITED ELECTRON-SPIN RESONANCE IN $\text{Hg}_{1-x}\text{Cd}_x\text{Te}$

B. D. McCombe, R. J. Wagner, and G. A. Prinz
Naval Research Laboratory, Washington, D. C. 20390
(Received 18 May 1970)

Electric-dipole-excited conduction-electron spin resonance has been observed for the first time in the far infrared in the II-VI semiconductor $\text{Hg}_{1-x}\text{Cd}_x\text{Te}$. Circular polarization and intensity studies as a function of magnetic field unambiguously identify this transition. Electron g values are obtained for the $L=0$ Landau level at several magnetic fields.

We report in this Letter what we believe to be the first observation of the electron-spin resonance transition excited by electric dipole radiation in a semiconductor in the far infrared.

A number of years ago "combined resonance" transitions, i.e., electric-dipole-excited transitions involving a change in the spin state of the carriers, were theoretically predicted for semi-

conductors with large spin-orbit interaction either having a small energy gap^{1,2} (the nonparabolicity mechanism) or lacking a center-of-inversion symmetry^{3,4} (the inversion-asymmetry mechanism).

Reported experimental observations of electric-dipole-excited transitions involving a spin flip thus far include the pure spin-flip transition (ΔL